Synthesis,Surface Morphology, Optical Properties and Photocatalyst Activities of $TiO_2/ZnO/Fe_2O_3$ Nanocomposites.

Juliya Acha Parambil
Mes Kalladi College
Abdul Mujeeb V.M
University of Calicut
S. Zh. Karazhanov
Institute for Energy Technology: Institutt for energiteknikk
Jayaram Peediyekkal (jayarampnair@gmail.com)
MES Ponnani College https://orcid.org/0000-0003-4112-3309

Research Article

Keywords: Triple layer nanocomposite, photocatalysis, methylene blue degradation, photoluminescence, nanocomposites

Posted Date: September 8th, 2020

DOI: https://doi.org/10.21203/rs.3.rs-70935/v1

Abstract

The photocatalytic degradation of methylene blue in aqueous solutions is enhanced significantly by formulating multiphase TiO_2/ZnO/Fe_2O_3 nanocomposites. The photocatalytic activity of unary TiO_2, binary TiO_2/ZnO, and ternary TiO_2/ZnO/Fe_2O_3 compounds are compared and reported. Using TiO2/ZnO/Fe2O3, methylene blue degradation became rapid and the reaction followed first-order kinetics. The consequences of the phase transition, surface features, and optical properties are compared and elucidated. The reduced photoluminescence intensity and decreased optical band gap energy in tertiary compounds impose higher degradation of methylene blue under irradiation.

1. Introduction

In the last few decades, the wide ecological imbalances are created by the usage of toxic materials that are accumulated in the environment to a large extent, in this context, there needs a destructive mineralization process that roots out the pollutants from the ecosystem [1]. Among the various toxic materials that are being discharged into nature, the dyes released from the textile industry occupies the forefront position [2]. Methylene blue, a heterocyclic aromatic byproduct compound of the aforesaid can interact with the aquatic environment and thus harms the aquatic organisms by depleting the content of oxygen [3–4]. The heterogeneous photocatalysis method is the competent method for the degradation of hazardous materials in the environment through the production of excitons upon illumination [5]. Various photocatalysts have been designed for the past years. Despite their high photocatalytic performance, the high electron-hole recombination and absorption of light near the ultraviolet region observed in such systems limit their practical applicability. One of the strategies to overcome this shortcoming is to use coupled semiconductors. Several materials are reported in the binary versions metal oxides with degradation properties and recently the efforts have been taken to the development of ternary photocatalytic systems. Because in ternary systems, the probability of multi-excitons generation and suppression of the electron-hole recombination can be higher [6]. The potential gradient developed at the interface results in the higher photocatalytic activity. Scientists have conducted various studies on the binary system TiO_2/ZnO.The studies prove that coupling enhances the charge separation and modify the electronic properties of the catalyst material [7–8]. .Herein, we report the synthesis and effectiveness of a single composition of TiO_2, TiO_2/ZnO, and TiO_2/ZnO/Fe_2O_3 system for the photocatalytic degradation of methylene blue. To elucidate the properties we report the structural, morphological, and optical properties of the compounds.

2. Materials And Methods

High purity tetra butyl titanate (TBOT), zinc nitrate Zn(NO□)□.6H_2O, and ferric nitrate $Fe(NO)_3$.9H_2O and the analytic grade reagents ethanol and acetic acid were used for the sol-gel synthesis of the composite of TiO_2/ZnO/Fe_2O_3. 12.9 ml TBOT initially dissolved in 51.1 ml absolute ethanol under vigorous stirring and 8.7 ml acetic acid, 0.66 ml water, and 12.9 ml ethanol are added slowly until a yellow transparent

solution is formed. Secondly, in a mixed solution of 20 ml, absolute ethanol, 6.5 ml acetic acid, and 2.5 ml deionized water; $Zn(NO_3).6H_2O$ and $Fe(NO)_3.9H_2O$ is added in required amounts. This second solution mixed in the first solution drop-wise with vigorous stirring at least for two hours. After aging this for 48 hours, the prepared sol was dried at 100^oC for 12 hours and then calcined at 500^oC for 5 hours in a microwave muffle furnace to obtain the end product. The same method was repeated for the synthesis of TiO_2 and TiO_2/ZnO in the absence of corresponding metal oxide raw agents. 50 ml of prepared standard methylene blue with a concentration of 10^{-4} M and 0.2 g of calcined photocatalyst (TiO_2, TiO_2/ZnO, TiO_2 /ZnO/Fe_2O_3) was added to the dye solution and stirred in the dark for 30 minutes to maintain the adsorption-desorption equilibrium. This is placed in, LZC-4X- Luzchem photo reactor provided with a bead and exposed to UV light for photocatalytic reaction measurements. The reaction was monitored by withdrawing 3 ml aliquots at an interval of 20 minutes. After degradation, the solution was centrifuged to eliminate the effects of scattering before the evaluation of the photocatalytic activity. The same experiment was conducted in direct sunlight with the most active catalyst. The intensity of sunlight at an interval of five minutes was measured using LUXMETER (LX-103). To characterize the materials optically UV-Vis DRS measurement was done using JASCO V-750 spectrophotometer and photoluminescence by JASCO Spectrofluorometer (FP-8300). BET surface area, pore-volume, and pore diameter were analyzed by BELSORP-max, automatic gas adsorption measuring unit for gas adsorption, vapor adsorption, and chemisorption. The diffraction patterns for X-ray diffraction analysis were recorded on Bruker AXS D8 advance diffractometer using Cu-Kα radiation (λ = 1.5406A0). The TEM analysis of the catalyst was performed on a JEOL/JEM 2100 transmission electron microscope.

3. Results And Discussions

3.1 Structural analysis

The nanocomposites formation is initially assessed by recording the XRD pattern [Fig. 1]. The diffraction peaks at 2θ = 25.39°, 37.85°, 48.11°, 62.76°, 69.05°, and 74.98° are the reflections of the (101), (004), (200), (204), (116), and (215) planes, respectively, originated from the anatase phase of TiO_2. While, 2Θ at 27.50°, 36.14°, 41.30°, 44.16°, 54.37°, 56.69°, 64.12° and 69.87° corresponds to the (110), (101), (111), (210),(211),(220),(310) and (312) plane of rutile phase of TiO_2[9]. The mixed-phase growth of TiO_2/ZnO was identified with the wurtzite hexagonal planes at 31.80°, 34.50°, 36.20°, 47.60°, 68.00° , 62.90° and 68.10° along with the prominent TiO_2 phase planes [10]. Apace with TiO_2/ZnO planes, reflections at 23.99°, 30.30°, 32.87°, 35.42°, 40.53°, 49.05°, and 61.90° are from the hematite phase of Fe_2O_3 [11]. These peaks confirm the formation of TiO_2/ZnO/ Fe_2O_3 composites and the broad intense peaks are substantiating evidence for the growth of nano-sized grains, this speculation is established with the grain size calculations performed by Scherrer equation [12] [Table. I]. The dislocation density has been calculated through Williamson and Smallman's formula [Table I].

Table.I. Average grain size calculated from the Scherrer equation and dislocation density from Williamson-Smallman's formula as well as the BET results, regression coefficient and rate constant of TiO_2, TiO_2/ZnO and TiO_2/ZnO/Fe_2O_3.

Compound	Avarage Grain Size (nm)	Dislocation Density x$10^{16}m^2$	BET surface area (m2/g)	Pore volume (cm3/g)	Regression coefficient (R^2)	$K_{app}(min)^{-1}$
TiO_2	22.53	0.20	29.1	0.029	0.99	0.007
TiO_2/ZnO	22.80	0.19	43.7	0.049	0.99	0.01
TiO_2/ZnO/Fe_2O_3	24.26	0.17	78.5	0.1335	0.93	0.02

3.2 Surface Morphology: Transmission Electron Microscopy and Brunauer–Emmett–Teller analysis

Figure 2 displays TEM and HRTEM images and SAED ring patterns for the surface topography of TiO_2, TiO_2/ZnO, and TiO_2/ZnO/Fe_2O_3. The low magnification images obtained from TEM results are presented in the first and second rows of the figure. The images divulge aggregated growth of particles in semi-globular shape, in the bilayer and triple layer composites. The shapes of particles are unaltered with roughly in the spherical shape. However, the average particle size obtained for TiO_2, TiO_2/ZnO, and TiO_2/ZnO/Fe_2O_3 were 19.1, 54.4, and 26 nm respectively. From the high-resolution TEM image the gap between two fringes in TiO_2, TiO_2/ZnO, and TiO_2/ZnO/Fe_2O_3 were obtained and are 0.27nm and 0.25 nm, these are indexed as (100) and (111) planes correspond to ZnO and Fe2O3 respectively [Fig. 2h and 2i]. The measurements obtained from the SAED rings for the three samples are consistent with the results of the XRD pattern. The surface-to-volume ratio obtained from BET measurements for TiO2, TiO_2/ZnO, and TiO_2/ZnO/Fe_2O_3 is 29.1, 43.7, and 78.5 m^2/g, respectively. The specific surface area has a pronounced effect on photocatalytic activity. The BET results indicate that the presence of Zn^{2+} and Fe^{3+} ion has significantly influenced the increase of the surface area of the samples. This is expected to activate more sites on the surface of the catalyst and thus to improve the photocatalytic activity [13].

3.3 UV-Visible Spectroscopy and Photoluminescence spectra

The UV-Visible spectra of TiO_2, TiO_2/ZnO, and TiO_2/ZnO/Fe_2O_3 nanosystem is represented in Figure 3a. The spectra of TiO_2/ZnO is slightly red-shifted in comparison with the spectra of bare TiO_2, this is further redshifted when the tertiary ionic system is formed. This is because of the presence of impurity levels spawn between the conduction band and valence band of TiO_2 as the Ti^{4+} either replaced by Zn^{2+}/Fe^{3+} ions or the at the interstitials and thus resulted in an altered band structure [13]. The prominent transition observed ≅ at 480 nm is the d→d (T2g →A2g) transition [14-15]. The optical band gap energies are estimated from the Kubelka-Munk re-emission function [15] and the corresponding values are 3.17eV,

3.07eV, and 2.9eV for TiO2, TiO2/ZnO, and TiO_2/ZnO/Fe_2O_3 respectively [Figure. 3b]. The reduction of the bandgap is expected and it is common for composite/hybrid materials consisting of two or more compounds with different bandgaps. The hybrid structure tune the energy band diagram by altering the valance band and conduction band entirely different from that of individual compounds and this will modulate optical properties with prominent influences the electronic charge exchange. Bandgap reduction is accompanied by enhancing the light absorption capability, which is beneficial for advancing photocatalytic properties of the composite. Figure.3(c) displays the PL spectrum of TiO_2, TiO_2/ZnO, and TiO_2/ZnO/Fe_2O_3, which is directly related to the electron-hole recombination and strongly influences the efficiency of photocatalysis. High PL intensity is expected to correspond to low photocatalytic efficiency. The materials exhibited two broad PL emission signals at 485 and 525 nm. The signal at 485 nm is due to the surface oxygen vacancies and emission at 525nm is due to the localized F+ centers on the surfaces of compounds [15-17]. The surface oxygen vacancies will act as charge trapping centers and prevent the electron-hole recombination. The order of emission intensity of the PL spectra is obtained in the following order TiO_2> TiO_2/ZnO>TiO_2/ZnO/Fe_2O_3. The decrease of PL intensity indicates the lower radiative recombination rate of photogenerated electron-hole in the composite. Because of possible efficient charge transport and separation due to beneficial conduction and valence band alignments.

3.4 Photocatalytic activity

Degradation of $1x10^{-4}$M methylene blue (MB) solution has been studied to test the photocatalytic performance of the composite TiO_2/ZnO/Fe_2O_3. Photocatalytic degradation of MB took place within 150 minutes [Fig. 4(a)]. The sunlight irradiation using the same catalyst the complete mineralization was achieved in 210 minutes, and its corresponding absorption spectra is indicated in Fig. 4(b). Evaluation of the photocatalytic dye degradation experiment was performed using the equation lnC0/C=kt. The photocatalysis followed the first-order kinetics. The estimated rate constant and regression constants are presented in Table. I. The degradation efficiency is calculated using the following equation [18-20].

Degradation percentage = ((A0-At)/A0) ×100%.

Here, A0 and At are the absorbance of methylene blue at the time of 0 and t respectively [18-20]. From this study, we have evaluated the photocatalytic performance of the composites. TiO_2-based photocatalyst exhibited the lowest performance. The composite TiO_2/ZnO showed larger efficiency whereas the three-layer composite TiO_2/ZnO/Fe_2O_3 exhibited the largest efficiency. The improved photocatalytic activity of TiO_2/ZnO/Fe_2O_3 can be mainly due to the reduced bandgap, enhanced optical absorption, more efficient charge transport, and separation.

3.5 Mechanism

The reason for the advanced photocatalytic process by the double and triple layer composites can be explained in the following way: Photogenerated electrons will migrate from the conduction band of ZnO to the conduction band of TiO_2 as the conduction band and valence band edges of ZnO is slightly higher

than that of TiO_2 [22-24]. In the case of Fe_2O_3, the conduction band and valence bands are placed between those of TiO_2 [22-25]. Hence these electrons continue to transfer to the conduction band of Fe_2O_3. At the same time, the holes from the valence band of TiO_2 are transferred to the valence band of Fe_2O_3 enhancing the effective spatial charge separation. Thus Fe_2O_3 acts as a recombination center making available the rest of electrons and holes in the valence band of TiO_2 and conduction band of ZnO respectively for dye degradation. Both the electrons and holes play a vital role in the degradation of methylene blue. The holes react with water molecules adsorbed on the surface to produce hydroxyl radicals whereas the photogenerated electrons on reacting with the adsorbed oxygen produce superoxide ions. The hydroxyl radicals and superoxide ions can decompose the dyes. Thus, the ternary system act as an efficient photocatalytic system by inhibiting the electron-hole recombination.

4. Conclusion

Binary and ternary metal oxide nanocomposites of TiO_2/ZnO and TiO_2/ZnO/Fe_2O_3- compositions have been successfully synthesized by incorporating TiO2, ZnO, and Fe_2O_3 by sol-gel method. The synthesized samples were subjected to various studies to depict its photocatalytic performance in methylene blue degradation. X-ray diffraction study confirms the mixed growth of metal oxide powders in multiphase and hence the compound in the composite category. The transmission electron microscopy and Brunauer–Emmett–Teller analysis implicit the growth nanoparticles and as the number of cations increases the surface area improved predominantly. It is inferred from the study that TiO_2/ZnO/Fe_2O_3 nanocomposite possesses visible light sensitivity, enhanced charge separation, and high surface area than the other two compound systems. The aforesaid factors shaped TiO_2/ZnO/Fe_2O_3, a far superior candidate than the bare TiO_2 and TiO_2/ZnO in the photocatalytic performance of methylene blue degradation. The complete demineralization of the dye in the presence of UV light was achieved within 150 minutes is one of the major findings of the study alongside with the degradation of the same concentration of the dye in direct sunlight within 210 minutes. The advanced photocatalytic performance has been explained by a reduced bandgap, enhanced sunlight absorption, and charge separation of the triple-layer TiO_2/ZnO/Fe_2O_3 and two-layer and TiO_2/ZnO composites than TiO_2.

Declarations

Acknowledgments:

P Jayaram acknowledges the DST –FIST level-0 program running in MES Ponnani College and SZK acknowledges INTPART project 309827 from the Research Council of Norway.

References

1. *Chintan Pathak et al, Journal of Environmental Pollution(2011), 2,08-10,*
2. *H. Ehrampoush et al, Australian Journal of Basic and Applied Sciences (2010) 4, 4279-4285.*

3. *Rafatullaha et al, Journal of Hazardous Materials (2010) 177 ,70–80*
4. *Abbasi et al, J. Hazard. Mater. (2008) 153, 942–947*
5. *Zaghbani et al, Desalination (2008) 222 ,348–356*
6. *Zaghbani et al, Desalination (2008) 222 ,348–356.*
7. *Janitabar-Darzi et al,Journal of Alloys and Compounds 486 (2009) 805–808*
8. *Giuseppe Marcı et al,J. Phys. Chem. B (2001) 105, 1033-1040*
9. *Jing He et al, Molecules 2019, 24, 2996.*
10. *Lin Lin et al, Nanoscale, 2013, 5, 588-593*
11. *Abdelmajid Lassoued et al, Results in Physics, Volume 7, 2017, Pages 3007-3015*
12. *Jayaram et al Physica B: Condensed Matter 501, 2016, 140–145*
13. *Intao Tian et al, Surface and Coatings Technology (2009) 204,723-730)*
14. *M. Riyas et al, Materials Letters 273 (2020) 127925*
15. *Dhayanantha Prabu Jaihindh et al,RSC Adv., 2018, 8, 6488-6501*
16. *Min Wei et al, Molecules 2017, 22, 950*
17. *Jing He et al, Molecules 2019, 24, 2996*
18. *Jasmin-Matheld Abdou et al, J.Chem.Phys.152, 064701(2020).*
19. *Jyoti Prakash Dhal et al, RSC Adv, (2015)5, 58072 –58083*
20. *C. Yu et al, Environ. Sci. Technol. 7 (2003) 2296,*
21. *Shwetharani et al, Catal. Sci. Technol., (2019)9, 12 –46*
22. *Khadija Munawar et al, RSC Adv., (2017)7, 15885 –15893*
23. *Xinjuan Liu et al Journal of Colloid and Interface Science (2013) 394 ,441–444*
24. *Simin Janitabar-Darzi et al, Journal of Alloys and Compounds (2009) 486, 805–808*
25. *Jingqun Gao et al, Desalination (2011) 268, 68 –75*

Figures

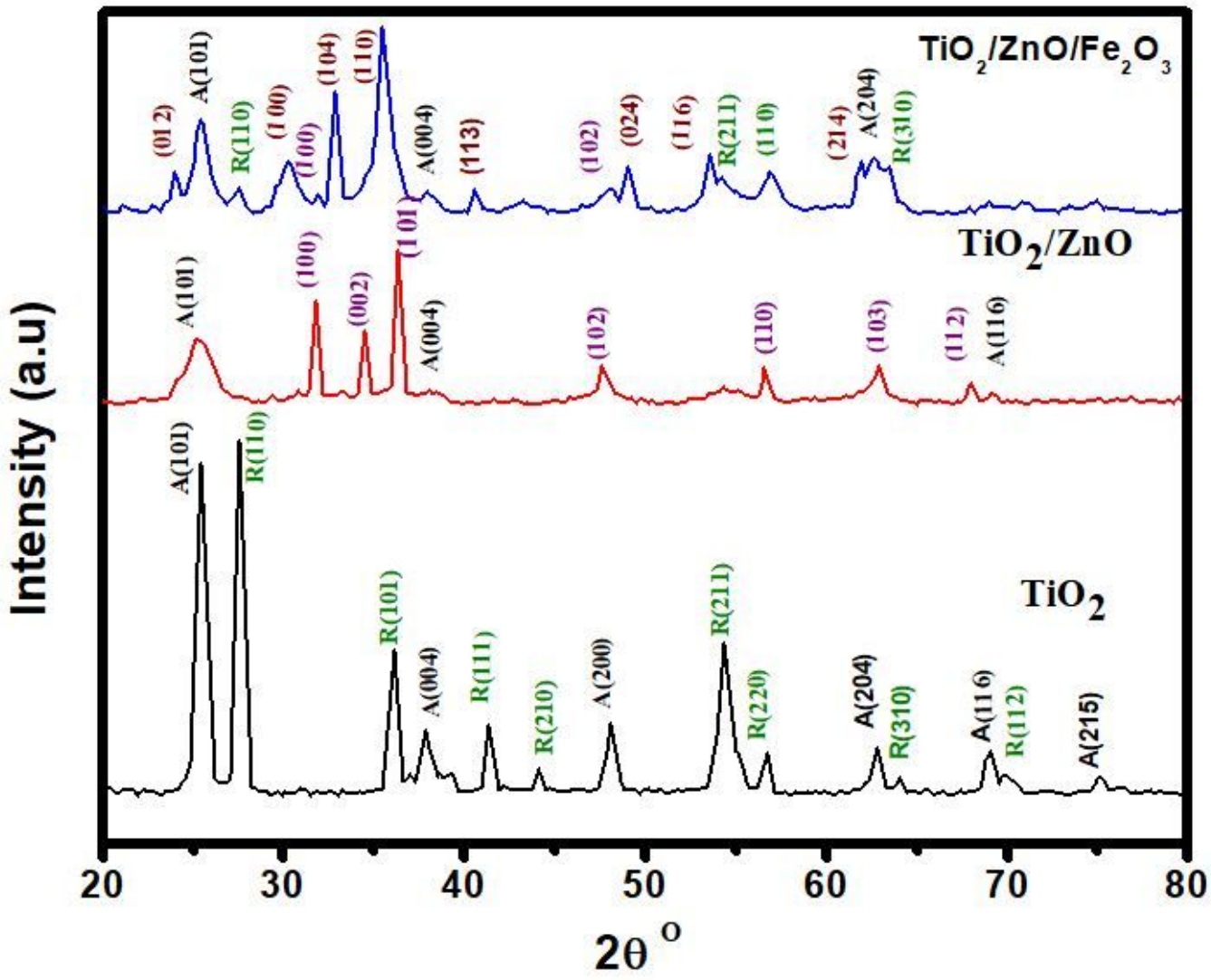

Figure 1

X-ray diffraction pattern of the compounds indicating the multiphase growth of nanoparticles.

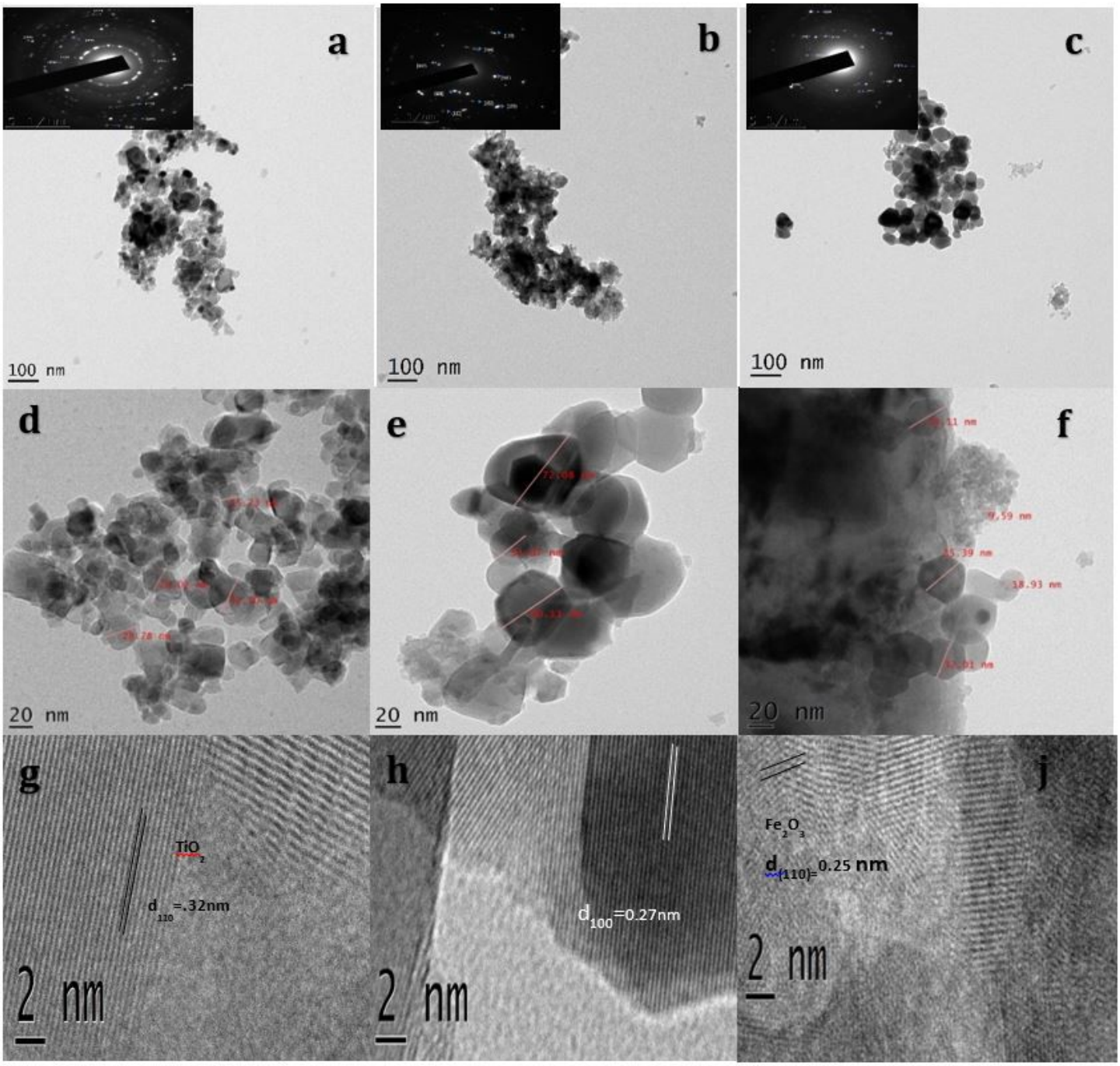

Figure 2

TEM images of (a) TiO2 (b) TiO2/ZnO (c) TiO2/ZnO/Fe2O3, inset shows seed images of corresponding particles. In second raw, low magnification TEM images of (d) TiO2 (e) TiO2/ZnO (f) TiO2/ZnO/Fe2O3. Third raw high magnification TEM images of (g) TiO2 (h) TiO2/ZnO (i) TiO2/ZnO/Fe2O3.

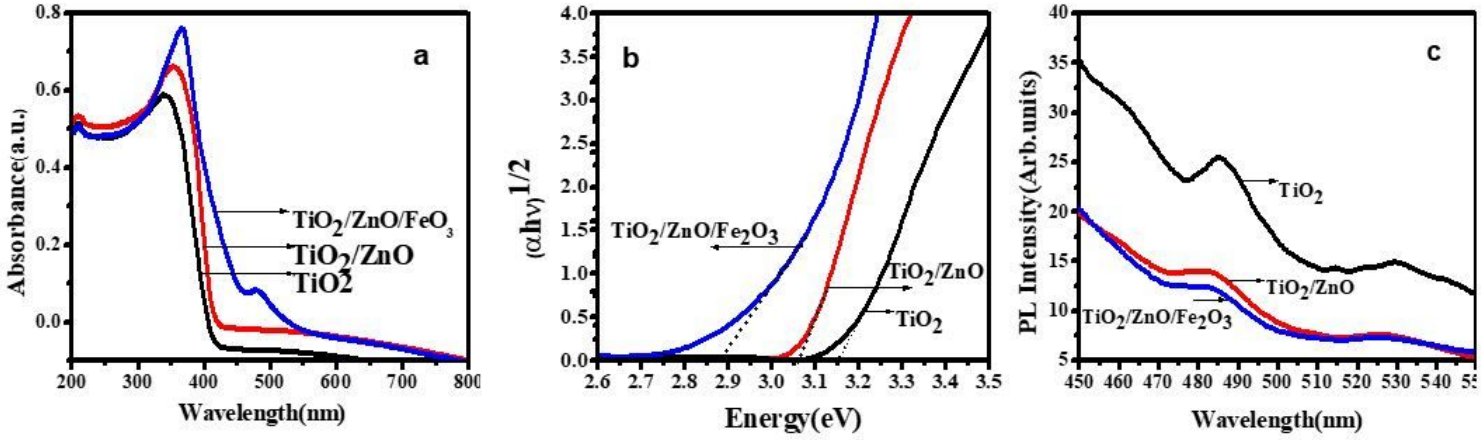

Figure 3

(a) UV-Vis Spectra of the samples recorded in Diffuse Reflectance Mode (b) The optical band gap energy determined by using Kubelka-Munk theory (c) The photoluminescence spectra of the samples

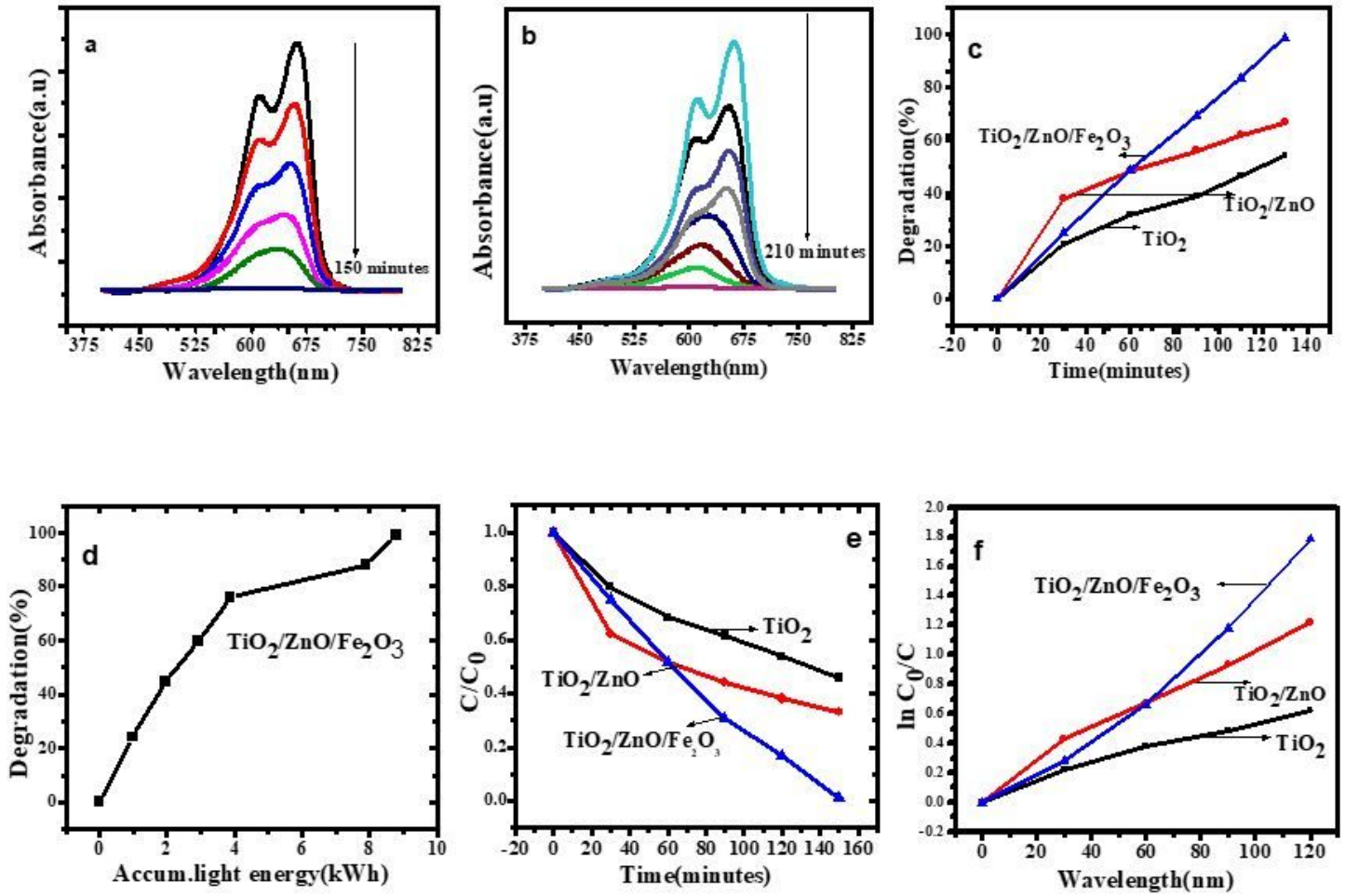

Figure 4

UV Absorption Spectra of photocatalytic degradation of methylene blue in the presence of (a) UV light irradiation (b) sunlight irradiation (c) percentage of degradation of methylene blue under UV irradiation and (d) the same for sunlight irradiation (e) C/C0 versus time of methylene blue degradation under UV irradiation (f) lnC/C0 versus time of Methylene blue degradation under the UV irradiation.